Probing the Acid Strength of Brønsted Acidic Zeolites with Acetonitrile: An Atomistic and Quantum Chemical Study

Alexandra Simperler,[†] Robert G. Bell,*[,†] Martin D. Foster,[†] Aileen E. Gray,[‡] Dewi W. Lewis,[‡] and Michael W. Anderson[§]

Davy Faraday Research Laboratory, The Royal Institution of Great Britain, 21 Albemarle Street, London W1S 4BS, United Kingdom, Centre for Theoretical and Computational Chemistry, University College London, 20 Gordon Street, London WC1H OAJ, United Kingdom, and UMIST Centre for Microporous Materials, Department of Chemistry, P.O. Box 88, Manchester M60 1QD, United Kingdom

Received: June 12, 2003; In Final Form: March 17, 2004

Computational chemistry methods have been used to study factors contributing to the Brønsted acidity of seven high-silica zeolites. For each structure type, one representative Brønsted site was chosen based on a systematic minimization protocol. Calculations of the ν(OH) stretching frequencies and the gradient norm of the electric potential at the proton site were performed. From these values, the sequence in order of decreasing intrinsic acidity, i.e., proton affinity, in the absence of any adsorbed base molecule, was established as follows: MFI > MOR > MTW > CHA > FER > TON > FAU. In the second phase of the calculations, an acetonitrile molecule was introduced into each zeolite using the Monte Carlo docking method, followed by DFT cluster optimizations. Acidity was related to the strength of the O−H···N hydrogen bond, which was characterized by a number of geometric parameters, and by adsorption energy. From the DFT calculations, the ranking of zeolites in order of decreasing hydrogen bond strength was MFI > FAU > MOR > MTW > CHA > FER > TON. The enhanced H-bond strength in FAU, relative to the other zeolites, is interpreted in terms of the large free volume of its pore system, which allows the acetonitrile to interact with the acidic site with minimal steric hindrance. Conversely, MFI maintains its position as the most acidic zeolite, despite the fact that acetonitrile adsorbs less favorably than in large-pore zeolites. In discussing the acidity actually encountered by a molecule within a given zeolite, it is therefore necessary to consider not only the intrinsic acidity of the Brønsted proton but also constraints due to the particular pore topology, which strongly influence the geometry by which a basic molecule is able to interact with the acid site.

1. Introduction

Aluminosilicate zeolites containing Brønsted acidic protons have major importance as catalysts in a host of commercially important processes, due to the large number of reactions which are initiated or promoted with a proton transfer. The catalytic performance of these types of zeolites is strongly governed by the acid "strength" of the protons as well as by their numbers, the latter largely determined by the Si/Al ratio. As discussed below, it is possible to conceive of a number of definitions of Brønsted acid strength. However, in the most general terms, one would state that the more acidic the proton, the higher the probability of its being transferred to the reacting species.

An illuminating approach to investigating the activity, or acidity, of these protons has been simply to consider protonated sites within the bare, unloaded zeolite. This has led to a number of studies,[1−8] both experimental and theoretical, of proton mobility and of deprotonation energies as methods of quantifying acidity. In this context, increased acidity can be said to be related to greater proton mobility and/or lower proton affinity. Furthermore, in the early 1990s the development of NMR techniques, for example magic angle spinning (MAS), two-dimensional techniques, and gradient techniques, allowed a closer insight into the nature of different hydroxyl groups present in a zeolite.[9−12] In studies of this type on unloaded zeolites, reference is often made to "intrinsic" acidity. This can also be thought of as corresponding (inversely) to the proton affinity of the zeolite, the main influences on which are simply local framework geometry and composition.

However, one could also argue that the concept of Brønsted acidity is meaningless in the absence of a proton acceptor. This is especially pertinent in the case of zeolites, where the approach of a proton acceptor to the acid site is strongly affected by the pore topology. Therefore, an alternative approach involves the interaction of probe molecules with the Brønsted sites to investigate the actual acidity experienced by a given molecule within a particular pore system. Many theoretical[13−22] and experimental studies, the latter using NMR, IR, and microcalorimetry,[23−35] have concentrated on these interactions. The ammonia molecule has played an important role in many such experiments. It forms ammonium on Brønsted sites and ammonia on Lewis acid sites, and thus, in addition to giving information about the strength of acidity, it can be used to estimate the amounts of Lewis and Brønsted acid sites contained in a zeolite. Moreover, ammonia can uniquely be used in IR, NMR, and temperature-programmed desorption (TPD)[36−43] studies. However, it is a strong base, invariably protonated at Brønsted sites, and thus not able to discriminate between sites of varying acidity. If some scaling of acid strength is desired, weaker bases are more appropriate as probes. Acetonitrile[44−56]

* To whom correspondence should be addressed. E-mail: rob@ri.ac.uk. Fax: +44 20 7629 3569.
[†] The Royal Institution of Great Britain.
[‡] University College London.
[§] UMIST Centre for Microporous Materials.

10.1021/jp035673t CCC: $27.50
Published on Web 05/06/2004

is a very good weak base for testing the acidity, as its main interaction with a Brønsted site is a hydrogen bond interaction of the type zeolite-O−H···N≡C−CH_3. Inter- or intramolecular O−H···N bonds are important features in organic and biochemistry, and a very popular method to characterize their strength is to equate the ν(OH) and the ν(C≡N) stretching frequency shifts with the hydrogen bond strength. The more ν(OH) is shifted toward lower frequencies, or ν(C≡N) toward higher, the stronger the interaction may be said to be. A combined theoretical and infrared study of intramolecular O−H···N hydrogen bonds[57] showed that interaction energies derived from density functional calculations correctly predict the trends found by experiment. Here we transfer this approach to investigate the intermolecular hydrogen bonds in the zeolite−acetonitrile complexes and hence to characterize the acid strength of the zeolites.

In the present paper, we report the results of two sets of calculations. In the first, classical atomistic calculations are used in a detailed study of the relative stability of Brønsted acid sites in seven unloaded high-silica zeolites. For each framework type, one structure (i.e., Al−OH− configuration) was chosen for further investigations. The intrinsic acidity of the seven selected structures was gauged by calculating both the ν(OH) stretching frequencies and the gradient norm of the electrostatic potential at the proton site. In this case, the ν(OH) frequency serves as an indicator of acid strength in the unloaded zeolite and enables direct comparison to be made with experimental data.

Following this, quantum chemical calculations were carried out on clusters representing the individual Brønsted sites in the chosen structures, both "bare" and interacting with acetonitrile. The cluster models were carefully selected to model the Brønsted site as well as significant portions of the neighboring zeolite pore system. A range of geometries and energies are presented and discussed. Although we are unable to calculate vibrational frequencies in these cases, since the clusters cannot be fully optimized, acidity in the sorption complexes is instead characterized from the hydrogen bond strength, as measured by the O−H and O−H···N distances. Here, we use the hydrogen-bond strength as a descriptor of acidity, with greater hydrogen bond strength being related to stronger acidity.

2. Zeolite Models and Methods

The starting geometries for the seven zeolite structure types were taken from the Cerius4.0[58] library. Figure 1a−f illustrates the zeolite structure types, showing only the connectivity of T sites, with the darker region indicating the clusters chosen for quantum chemical calculations. Figure 1g−n shows the corresponding clusters with acetonitrile hydrogen bound to the acid proton (optimized as described below) and the numbering of T sites and oxygen atoms according to Calligaris et al.[59] for CHA, Olson[60] for FAU, Vaughan[61] for FER, Olson et al.[62] for MFI, Alberti et al.[63] for MOR, Fyfe et al.[64] for MTW, and Highcock et al.[65] for TON, respectively. In each case, the terminating hydroxyl groups have been omitted for clarity.

CHA[59] (Figure 1a) has a framework characterized by double six-membered rings linked by tilted four-membered rings surrounding large ellipsoidal cavities that can be entered via eight-membered rings. It has only one crystallographically distinct T site. Catalysts of this framework type are able to convert methanol into light alkenes.

FAU[60] (Figure 1b) also has a uninodal framework. Its sodalite units (i.e., truncated cubooctahedra) are connected by double six-membered rings giving rise to the characteristic supercages, interconnected through 12-ring pores.

FER[61] (Figure 1c) has four different T-sites. It contains 10-membered ring channels running parallel to the crystallographic [001] direction, intersecting with eight-membered ring channels parallel to the [010] direction. The 10-membered rings are composed of T atoms in sites T2, T3, and T4, whereas eight-membered rings are composed of atoms in T2 and T4 sites. T1 sites are exclusively located in six-membered rings. It may be used as catalyst in the isomerization of *n*-butene.

MFI[62] (Figure 1d) has 12 different T-sites and its three-dimensional channel system consists of straight 10-membered ring channels running parallel to [010] and sinusoidal channels running parallel to [100].

MOR[63] (Figure 1e) has four symmetrically independent T sites and contains two different types of cavities: a 12-membered ring channel running parallel to the [001] direction and "side channels" in the main channel wall orientated in [010] direction and circumscribed by eight-membered rings.

MTW[64] (Figure 1f) has seven crystallographically distinct T-sites and unidirectional 12-membered ring channels which do not intersect.

TON[65] (Figure 1g) has four independent T atoms and 10-membered ring channels parallel to [001]. All illustrations in Figure 1 have employed POV−Ray.[66]

For each structure type, the first aim was to identify a representative Brønsted site, based on a type of global minimization protocol. The main selection criteria were the thermodynamic stability of the structure and also, importantly, the accessibility of the acid proton. An initial computer procedure, *MAGIC*,[67] performed the task of substituting each of the symmetrically distinct T atoms with an Al atom and placing a proton on each of its four adjacent bridging oxygen atoms. The hydrogen is placed at 1.0 Å distance from the oxygen and in the plane of the Al−O−Si bond, which is a highly accurate starting point for minimization and minimizes the risk of finding a local minimum when optimizing the structure. For a structure with n different T atoms, $4n$ starting configurations will thus be produced for lattice energy minimization. Our aim was to look at a dilute level of acid site concentration, hence the choice of one site per unit cell. Since minimizations were carried out using periodic boundary conditions, with the generally accepted unit cells for each zeolite, the Si/Al ratios for each zeolite were therefore 11 for CHA, 191 for FAU, 35 for FER, 95 for MFI, 95 for MOR, 55 for MTW, and 23 for TON, respectively. The minimizations themselves were carried out using GULP.[68] The potentials used were those described by Schröder and coworkers,[69] including the highly accurate Sanders et al. silica potential[70] and the Al−O potential derived by Catlow et al.[71] The O−H bond was represented by the Morse potential terms originally derived by Saul et al. from ab initio calculations.[72] The shell model is included to allow for the polarization of framework oxygen. Minimizations were carried out under constant pressure conditions; that is, unit cell parameters were allowed to vary as well as atomic positions. Those structures resulting in the lowest lattice energies were taken as the most thermodynamically favored. However, structures were excluded if the proton site was found to be inaccessible from the pore volume (as was the case for some of the FAU, MTW, and TON structures). Phonon frequency calculations were also performed in GULP, and the frequency values as well as the gradient norm at the proton site, $|E|_H$, have been extracted. Frequencies were subject to a -150 cm^{-1} anharmonicity correction.[69]

The GULP minimized structures were then further used as the starting points for Monte Carlo docking[73] calculations in which one acetonitrile molecule was introduced into each zeolite.

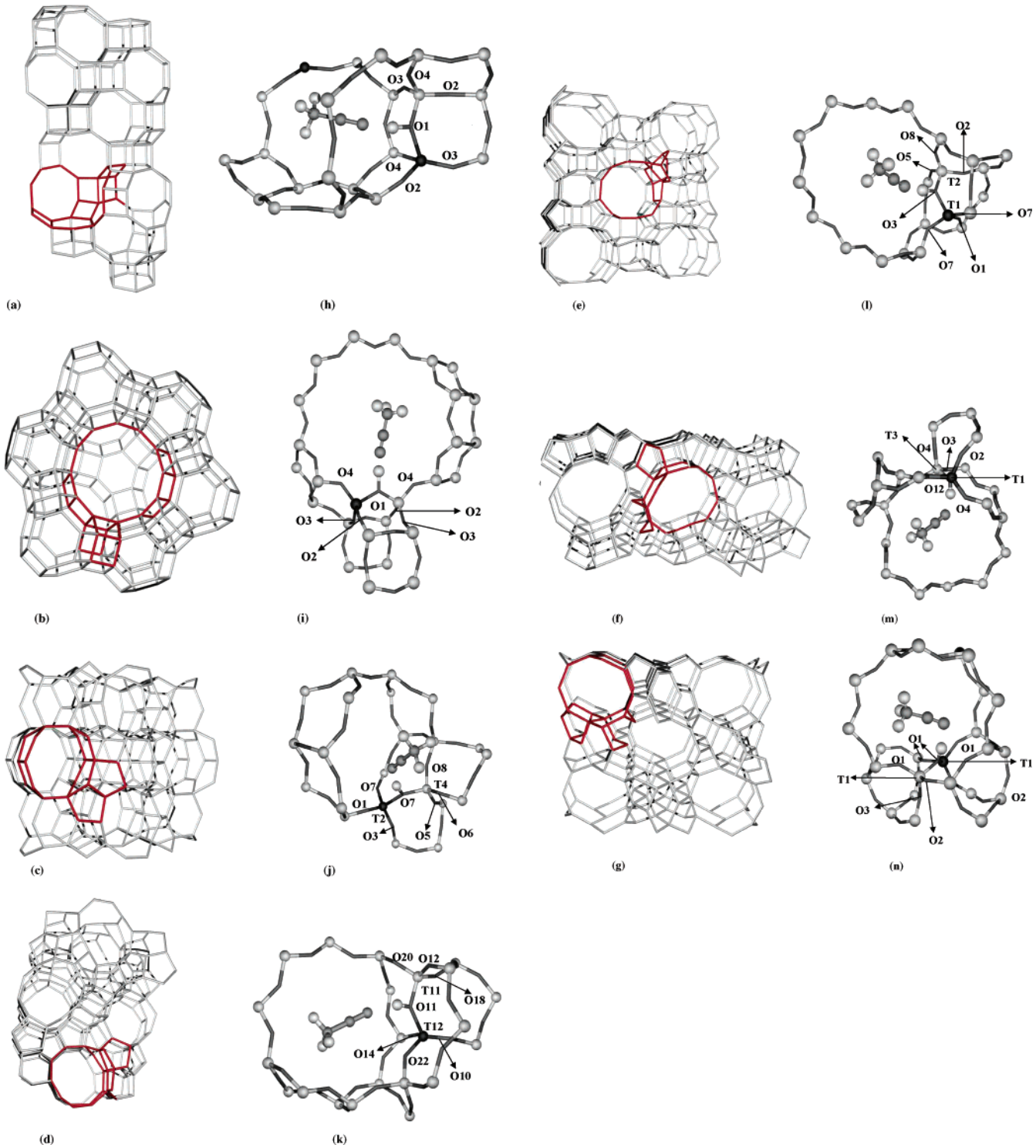

Figure 1. Drawings of the structure types (a) CHA, (b) FAU, (c) FER, (d) MFI, (e) MOR, (f) MTW, and (g) TON. The structure types are simplified by presenting the T−T connectivity only, with the dark part denoting the cluster. The clusters themselves are presented adjacent as h−n, and for the sake of clearness the terminating hydroxy groups are not shown.

The *cff91_czeo* force field[74] was used. In each case, low-energy docked configurations for the molecule in the vicinity of the acid site were obtained, and these in turn provided initial geometries for DFT cluster calculations. The clusters, including the acid site and adsorbed acetonitrile molecule, were chosen so as also to include a sufficient representation of the surrounding zeolite channel system (see Figure 1h−n). The numbers of atoms in the clusters varied between 116 and 137 atoms. During the DFT optimizations, only acetonitrile and the first coordination sphere around the Brønsted site, $\equiv O_3Si-(OH)-AlO_3\equiv$, was allowed to relax while all of the other atoms are kept fixed at the positions obtained from the force field calculations. Keeping the peripheral atoms of the cluster fixed is essential to avoid an unrealistic collapse of the pore structure. Moreover, with the framework already having been minimized in the presence of the acetonitrile molecule using an accurate force field, it was deemed unnecessary to optimize more atoms in the DFT calculations, which would have involved a much greater computational expense. A corollary to this approximation is that it is not possible reliably to calculate vibrational spectra

TABLE 1: Sequences of the Brønsted Sites in Order of Decreasing Stability[a]

CHA	**Al1−O1−Si1** (0) > Al1−O4−Si1 (2.27) > Al1−O3−Si1 (17.21) > Al1−O2−Si1 (23.96)
FAU	Al1−O3−Si1 (0) > **Al1−O1−Si1** (10.27) > Al1−O2−Si1 (25.75) > Al1−O4−Si1 (32.16)
FER	**Al2−O7−Si4** (0) > Al3−O8−Si4 (7.74) > Al3−O2−Si3 (9.92) > Al4−O6−Si4 (11.39) > Al4−O8−Si3 (12.04) > Al4−O5−Si4 (12.29) > Al3−O4−Si1 (15.92) > Al1−O4−Si3 (16.20) > Al2−O3−Si1 (16.83) > Al4−O7−Si2 (23.60) > Al1−O3−Si2 (29.67)> Al2−O1−Si2 (55.48)
MFI	**Al11−O11−Si12** (0) > Al7−O17−Si4 (7.09) > Al4−O17−Si7 (12.20) > Al3−O20−Si12 (12.36) > Al12−O20−Si3 (13.18) > Al3−O19−Si6 (14.78) > Al12−O11−Si11 (16.29) > Al1−O1−Si2 (17.73) > Al7−O7−Si8 (17.81) > Al8−O7−Si7 (18.68) > Al12−O12−Si8 (21.54) > Al8−O13−Si2 (22.20) > Al7−O22−Si11 (22.59) > Al8−O8−Si9 (22.72) > Al2−O6−Si6 (23.07) > Al5−O5−Si6 (23.66) > Al9−O9−Si10 (23.76) > Al2−O13−Si8 (24.66) > Al11−O10−Si10 (24.97) > Al2−O1−Si1 (25.05) > Al2−O2−Si3 (26.18) > Al6−O19−Si3 (26.64) > Al1−O15−Si10 (26.77) > Al9−O8−Si8 (27.03) > Al3−O2−Si2 (28.83) > Al10−O26−Si10 (28.93) > Al5−O21−Si1 (29.16) > Al3−O3−Si4 (29.38) > Al11−O22−Si7 (29.63) > Al4−O4−Si5 (29.69) > Al12−O24−Si12 (29.78) > Al1−O16−Si4 (29.84) > Al8−O12−Si12 (30.13) > Al10−O10−Si11 (30.88) > Al5−O14−Si11 (31.60) > Al5−O4−Si4 (32.22) > Al6−O5−Si5 (32.28) > Al9−O18−Si6 (32.47) > Al10−O15−Si1 (33.64) > Al1−O21−Si5 (33.64) > Al10−O9−Si9 (33.74) > Al9−O25−Si9 (34.15) > Al4−O16−Si1 (34.68) > Al4−O3−Si3 (35.97) > Al11−O14−Si5 (36.16) > Al6−O6−Si2 (39.07) > Al6−O18−Si9 (39.95) > Al7−O23−Si7 (44.63)
MOR	**Al1−O3−Si2** (0)> Al3−O1−Si1 (4.54) > Al1−O7−Si1 (5.83) > Al4−O2−Si2 (7.69) > Al3−O1−Si1 (11.05) > Al1−O1−Si3 (12.47) > Al3−O4−Si4 (12.91) > Al4−O2−Si2 (13.92) > Al1−O1−Si3 (14.64) > Al4−O4−Si3 (15.11)> Al2−O3−Si1 (15.94) > Al2−O5−Si2 (17.17) > Al2−O2−Si4 (17.34) > Al2−O8−Si2 (19.37) > Al3−O9−Si3 (20.93) > Al4−O10−Si4 (26.52)
MTW	Al6−O14−Si5 (0) > **Al1−O3−Si3** (4.15) > Al7−O7−Si7 (4.32) > Al4−O13−Si2 (5.56) > Al6−O8−Si5 (5.92) > Al2−O13−Si4 (9.26) > Al2−O5−Si4 (10.89) > Al5−O8−Si6 (11.47) > Al3−O3−Si1 (12.92) > Al3−O12−Si1 (17.12) > Al4−O5−Si2 (17.27) > Al1−O12−Si3 (18.66) > Al5−O14−Si6 (19.14) > Al3−O6−Si7 (26.56) > Al7−O11−Si6 (34.52) > Al5−O4−Si3 (34.79) > Al2−O1−Si1 (36.78) > Al6−O4−Si9 (36.89) > Al1−O2−Si2 (37.91) > Al1−O1−Si2 (37.99) > Al7−O6−Si3 (38.18) > Al3−O4−Si5 (38.59) > Al4−O10−Si5 (39.71) > Al4−O9−Si6 (39.75) > Al2−O2−Si1 (43.23) > Al6−O11−Si7 (44.24)> Al5−O10−Si4 (57.66)
TON	Al2−O22−Si2 (0) > (Al2−O22−Si2)′ (0.85) > Al3−O34−Si4 (1.66) > **Al1−O11−Si1** (8.89) > (Al1−O11−Si1)′ (10.02) > Al3−O43−Si4 (20.20) > Al4−O34−Si3 (20.98) > Al4−O43−Si3 (23.18) > Al1−O14−Si4 (27.14) > Al2−O23−Si3 (33.00) > Al2−O12−Si1 (35.56) > Al3−O23−Si2 (36.39) > Al1−O12−Si2 (41.66) > Al4−O14−Si1 (45.59) > (Al4−O14−Si1)′ (45.95)

[a] Bold print indicates the chosen site for subsequent quantum chemical investigations. In parentheses the energy difference [kJ/mol] to the lattice energy of the thermodynamically most stable structure is given.

without full optimization. Dangling bonds were saturated with hydroxy groups in such a way that the cluster remained charge neutral. The hydroxy groups were aligned away from the probe molecule and from each other, to avoid artificially induced hydrogen bond interactions. We refer to the whole series as clusters Z−A (Z = CHA, FAU, FER, MFI, MOR, MTW, and TON) when acetontrile is present. The corresponding clusters without the acetonitrile molecule are referred to as clusters Z. The clusters were optimized with the *DMol* program,[58] employing a PW91[75] density functional and the dnp basis set (i.e., a double numerical basis function with polarization functions, comparable to the Gaussian basis set 6-31G(d,p)[76]). Adsorption energies/hydrogen bonding energies were calculated as well as geometric parameters.

3. Results and Discussion

3.1. Localization of the Protonated Sites. Table 1 lists all of the possible Brønsted sites of the various zeolite structures in order of decreasing lattice energy, as calculated by GULP. In parentheses the lattice energy per unit cell (i.e., per site) with respect to the most stable structure is given. The results may be summarized as follows:

CHA. We find the lowest lattice energy with the acid proton on site O1 (Al1−O1−Si1) which is confirmed by other authors.[77,78]

FAU. The structure where O3 is protonated is the most stable. This is at odds with previous embedded quantum chemical calculations,[79] which predict O1−H to be the most energetically favorable. Nevertheless, we chose the O1−H site for further study since the O3−H proton points into a sodalite cage and is therefore not easily accessible. In IR and NMR spectroscopic studies protonation of O1 and O3 is mostly found, results which are also confirmed by other calculations.[80−82]

FER. Infrared studies[83] have identified T2 as the site with highest Al population, whereas a neutron powder diffraction study[84] determined two Brønsted sites in low-silica FER: T1-O4-T3 and T4-O6-T4. FER dehydroxylates easily and Lewis sites are frequently present as shown by an acetonitrile adsorption study.[85] The high-silica model which we use in our calculations has a Si/Al ratio of 35 and, according to this, the thermodynamically most stable structure is protonated on O7 with Al substituted on T2. At this site, the proton is pointing into the 10-membered ring channel.

MFI. We obtained Al11−O11−Si12 as the most energetically preferred site for protonation. Khaliullin et al.[86] assumed Al7−O17−Si4 to be the most stable, a site which comes second in our calculations. Modeling studies of water adsorption by Zygmunt et al.[87] employ the Al12−O24−Si12 site in their clusters, as do Brand et al.[88] Sierka and Sauer[1] have the proton on O7.

MOR. We found Al1−O3−Si2 to be the most stable protonated site. This is in agreement with LDA and GGA calculations.[89] A neutron diffraction study[90] of MOR with Si/Al ratios of approximately 5 and 10 identified O5, O6, O9, and O10 as the oxygen atoms to which H is likely to be attached, whereas a different structure refinement[91] locates the acid protons on O2 and O7 in the main channel and on O9 in the side pockets.

MTW. We have chosen Al1−O3−Si3 as the Brønsted site we want to investigate in MTW, rather than Al6−O14−Si5,

TABLE 2: Stretching Frequencies, ν(O−H), the Gradient Norm of the Potential at the Proton Site, $|E|_H$, and Bond Distances and Angles of the Brønsted Site, as Obtained from GULP Calculations

	ν(O−H) [cm^{-1}]	$\|E\|_H$ [VÅ^{-1}]	r(O−H) [Å]	r(O−Al) [Å]	r(O−Si) [Å]	r(H···Al) [Å]	r(H···Si) [Å]	∠(Al−O−Si) [°]	∠(Al−O−H) [°]	∠(Si−O−H) [°]
MFI	3580	13.25	1.002	1.919	1.685	2.282	2.377	139.9	97.8	122.3
MOR	3582	13.28	1.002	1.928	1.680	2.285	2.401	137.0	97.4	125.2
MTW	3593	13.40	1.001	1.872	1.724	2.381	2.369	133.7	108.0	118.3
CHA	3597	13.42	1.001	1.929	1.686	2.309	2.388	137.5	99.1	123.4
FER	3601	13.48	1.003	1.924	1.678	2.276	2.358	141.8	97.0	121.1
TON	3606	13.54	1.001	1.874	1.713	2.362	2.372	134.0	106.5	119.5
FAU	3621	13.70	0.999	1.921	1.685	2.382	2.389	131.4	104.8	123.7

the most stable one, in which H points into a six-membered ring channel and is thus inaccessible to molecules.

TON. We have chosen Al1−O11−Si1, which comes fourth in our stability ranking but is the first structure of which the proton site is accessible. The accessible Brønsted sites in order of decreasing stability are Al1−O11−Si1 > Al2−O23−Si3 > Al2−O12−Si2 > Al2−O23−Si3 > Al1−O12−Si2. Boronat et al.[92] found a different sequence, namely Al2−O23−Si3 > Al2−O12−Si2 > Al2−O23−Si3 > Al1−O11−Si1 > Al1−O12−Si2. In their calculations, they used the Schröder−Sauer potential,[93] which uses a quite different parametrization to our model, being derived from ab initio calculations. Table 2 lists selected geometric data as obtained by GULP lattice energy minimization. The bond lengths do not vary significantly between the different sites, the variation for each type of distance being about 0.1 Å in total. The spread of angles observed is close to 10°.

3.2. Intrinsic Acidity. The flexibility of the lattice, the electrostatic potential, and the electron distribution near the acid site are the main governing factors of the intrinsic acidity, i.e., the proton affinity of a bare Brønsted site. Infrared spectroscopy is an extremely powerful method of measuring the strength of O−H bonds, since this is essentially synonymous with the O−H stretching frequency, which can thus be related to the acid strength of the acid site. In previous work,[94−96] Sastre and Lewis, employing essentially the same modeling methods as used here, found a direct correlation between ν(OH) and the gradient norm of the electrostatic potential at the proton, emphasizing the importance of long-range effects as well as those of local environment. They also found a correlation between ν^2(OH) and the energy required to elongate the OH bond by 0.1 Å, essentially a component of the proton affinity. This relationship held for a number of different zeolite structure types, at the dilute limit of acid site concentration. In general, the protons in larger channels or cavities are held to be more tightly bound than those in smaller cavities, where more framework atoms are in close proximity. Sastre and Lewis however failed to find any correlation between ν(OH) and cavity size in their simulations, suggesting that all close nonbonded OH···O interactions need to be taken into account, not just those within the same cage.

In the calculations, we first define the potential gradient at the proton site, $\epsilon = q \int E \, dr$, where E is the negative gradient of the electrostatic potential and r is the displacement vector along the direction of the bond. If we consider now the gradient norm of the potential at the proton site, $|E|_H$, we have a measure of the shallowness of the potential at the proton site, whereby the smaller $|E|_H$ the more easily the proton may be removed.

Calculated ν(OH) and $|E|_H$ data are given in Table 2 in addition to the geometric parameters of the selected structures. The data are sorted in order of increasing ν(OH), i.e., starting first with the most acidic. In Figure 2 the ν(OH) frequencies are plotted versus $|E|_H$, and as we expect from previous work,[94−96] there is an extremely good correlation between the two sets of values (the relationship has been shown to be quadratic, but approximates to linearity over narrow ranges of ν[94]). However, when comparing the geometric measurements with ν(OH) and $|E|_H$, respectively, no significant trends are observed, which stands in contrast to the correlation between acid strength and Al−O−Si angle discussed by other authors.[5,8] If ν(OH) is taken as an indicator of acidity, then the Brønsted acid site in MFI is the most acid, whereas the one chosen in the FAU structure is found to be the weakest. On this basis, we thus predict the following sequence, in order of decreasing acidity, for zeolites with one Al atom per unit cell: MFI (95) > MOR (95) > MTW (55) > CHA (11) > FER (35) >TON (23) > FAU (191), where the numbers in parentheses indicate the Si/Al ratio.

Experimentally, IR measurements of these structures are quite complex since it is often difficult to deconvolute the broad OH bands into their individual components. For example, in two studies[53,85] the authors were able to assign particular regions to surface silanol groups and Brønsted acid OH groups in general. It was also possible for them to distinguish whether the acid OH groups point into a smaller or a larger cavity within a structure. Since we have deliberately modeled OH groups located in the larger pores, we will consider only frequencies which were assigned to such groups. The frequency of Brønsted OH in MFI (Si/Al = 12.6) was measured as 3612 cm^{-1} by

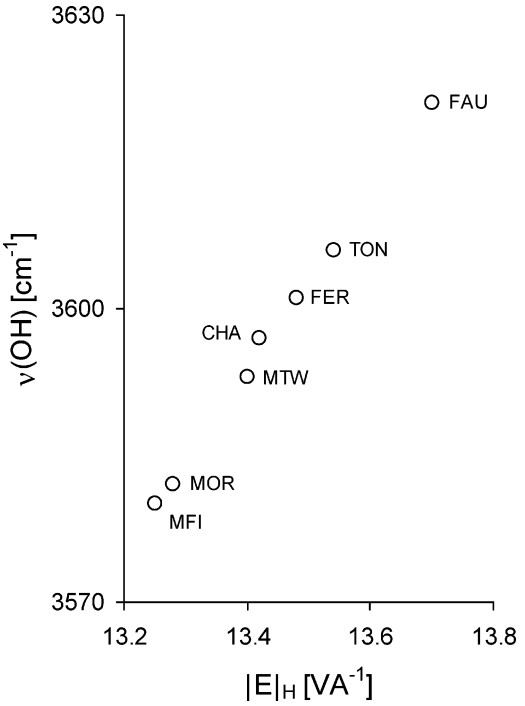

Figure 2. Plot of the ν(OH) stretching frequencies versus the gradient norm of the potential at the proton site, $|E|_H$, as obtained from atomistic calculations.

TABLE 3: Bond Distances and Angles of the Bare Brønsted Site (Upper Part) and of the Site in Interaction with Acetonitrile (Lower Part), as Obtained from Quantum Chemical Cluster Calculations[a]

	r(O−H) [Å]	r(H··N) [Å]	r(O−Al) [Å]	r(O−Si) [Å]	r(H···Al) [Å]	r(H···Si) [Å]	∠(C≡N···H) [°]	∠(N···H−O) [°]	∠(Al−O−Si) [°]	∠(Si−O−H) [°]	∠(Al−O−H) [°]	E_{ADS} [kJ mol^{-1}]
MFI	0.977		1.894	1.695	2.392	2.309			134.3	117.0	108.6	
FAU	0.975		1.884	1.699	2.472	2.323			125.6	118.1	116.0	
MOR	0.977		1.896	1.703	2.406	2.318			128.3	117.1	109.6	
MTW	0.976		1.919	1.714	2.462	2.329			127.1	112.4	117.3	
CHA	0.975		1.878	1.703	2.401	2.307			132.9	116.4	110.6	
FER	0.978		1.887	1.667	2.337	2.293			136.1	117.8	104.8	
TON	0.975		1.927	1.713	2.471	2.342			126.2	118.6	112.6	
MFI-A	1.067	1.443	1.854	1.661	2.373	2.270	146.8	177.8	134.4	111.9	105.5	−70.0
FAU-A	1.046	1.544	1.847	1.671	2.520	2.336	166.1	175.1	124.7	116.7	118.5	−80.3
MOR-A	1.039	1.558	1.857	1.672	2.472	2.338	161.9	170.1	128.4	117.3	114.3	−75.8
MTW-A	1.037	1.604	1.897	1.700	2.424	2.290	127.6	161.6	125.3	111.3	107.8	−75.7
CHA-A	1.033	1.583	1.850	1.680	2.453	2.282	151.0	166.2	131.7	112.3	113.6	−56.8
FER-A	1.025	1.629	1.859	1.648	2.403	2.257	139.9	164.4	136.1	113.1	109.5	−49.5
TON-A	1.009	1.735	1.905	1.698	2.462	2.358	105.3	167.7	126.0	119.0	111.6	−45.6

[a] The last column comprises the adsorption energies, E_{ADS}, calculated as described in text (Figure 4).

Wichterlová et al.,[85] with Jänchen et al.[53] obtaining 3610 cm^{-1} for a Si/Al ratio of 52. MFI is one of the more complex framework structures with 12 topologically distinct T-sites, and thus 48 possible Brønsted sites. In this case, infrared spectroscopy can determine quantitatively only the overall amount of Brønsted acidity and is unable to determine the precise location and type of the acid sites, other than whether they are located in a small or large cavity. Experimental data for the other zeolites under consideration, together with their assignments by the original authors, are summarized as follows (as above, numbers in parentheses following a three-letter structure code denote the Si/Al ratio).

MOR(7.7) was studied by Zholobenko et al.,[35] who assigned 3612 cm^{-1} to an acid OH located in the main channel. Czyzniewska et al.[97] found 3607 cm^{-1} for MOR (10.7).

MTW(23) also has a band at 3612 cm^{-1}, assigned to an acid OH in the main 12-ring channel of the structure.[32]

In **CHA**(16), Smith et al.[30] clearly distinguished between protonation on framework oxygen atoms O1, in the eight-ring window, (3603 cm^{-1}) and on O2, in a six-ring (3579 cm^{-1}).

FER(6.3) has a band at 3609 cm^{-1}, identified as due to a Brønsted OH located in the 10-membered ring channel.[26]

TON(25) has recently been studied,[23] with an OH stretch of 3598 cm^{-1} being found. This is a fairly low frequency for a structure with no small cavities.

FAU(20.7) has a band measured at 3623 cm^{-1}.[98]

The experimental sequence in order of decreasing "acidity" (i.e., increasing ν(OH)) may thus be written TON(25) > CHA(16) > MOR(10.7) > FER(6.3) > MFI(52) > MFI(12.6) = MOR(7.7) = MTW(23) > FAU(20.7). In comparison with the calculated infrared data, there are a number of points of agreement. In particular, FAU emerges consistently with the highest frequency, having the most open channel system. MFI and MOR(7.7) also have very similar frequencies in both experiment and model. Also the range of values of the frequencies tally quite closely. The main discrepancy lies in the fact that TON, CHA, and FER have the lowest frequencies experimentally and thus are out of sequence compared to the calculations (leaving aside the lower value for MOR). TON in particular has a significantly lower frequency, though we note that in our model we ignored the three lowest-energy proton sites as they were inaccessible from the main channel system. If these sites were in reality protonated, it would seem reasonable to suppose that, being in more confined positions, their OH frequencies would be lower. Other sources of discrepancy include the fact that many of Si/Al ratios differ between the model structures and experimental materials, which would influence both the numbers of proton sites as well as their immediate environment and the overall electrostatic field. Also we use only one acid site as the basis for our predictions whereas in the real zeolite, additional sites of similar acidity could easily be occupied, leading to the observation of average values.

3.3. Brønsted Acidity Probed by Acetonitrile. Our principal intention was to investigate the behavior of the selected Brønsted sites in the presence of an approaching molecule and thus to model a situation which is representative of intrazeolite chemistry. Table 3 comprises data from quantum chemical calculations of both the clusters Z and Z−A. The results for the different bond lengths in Z show changes from 0.003 to 0.149 Å, whereas the angles each vary by between 6 and 13°. Compared to the GULP results, the O−H bond lengths are shorter when calculated with the quantum chemical method, whereas the O−Al and O−Si bond lengths are very similar with both methods. Also the H···Si and H···Al distances are shorter when calculated with the DFT method, and the Al−O−Si and Si−O−H angles are smaller, although the Al−O−H angles are larger. There exist no recognizable trends within the geometry data of the Brønsted sites when comparing atomistic methods and DFT.

In Figure 3, the N···H−O distance is plotted versus the H−O bond length and we find an excellent correlation (r = 0.98). Both these distances characterize the hydrogen bond strength in this system, the longer the O−H distance, and the shorter the hydrogen bond length, r(N··H−O). When using this criterion to define the sequence of decreasing hydrogen-bond strength, the following series is obtained: MFI(Si/Al=95) > FAU(191) > MOR(95) > MTW(55) > CHA(11) > FER(35) > TON(23). When compared to the "intrinsic" acidity series, it is immediately obvious that the sequence is identical, except that the position of FAU changes dramatically from having the lowest intrinsic acidity to being the second most acid in the presence of acetonitrile. We suggest that, due to its large supercage diameter, FAU allows the acetonitrile to access the Brønsted site without any major steric hindrance, whereas for all of the other structures the acidity experienced by the molecule is mediated by the geometric constraints of the pore system. In general, the O−Al and O−Si bonds are respectively about 0.2−0.4 Å and 0.1−0.3 Å shorter when acetonitrile is adsorbed at the Brønsted site (see data for Z−A in Table 3). The distances between the acid proton and Al or Si show some variation, but without any clear trend. The Al−O−Si angles vary slightly;

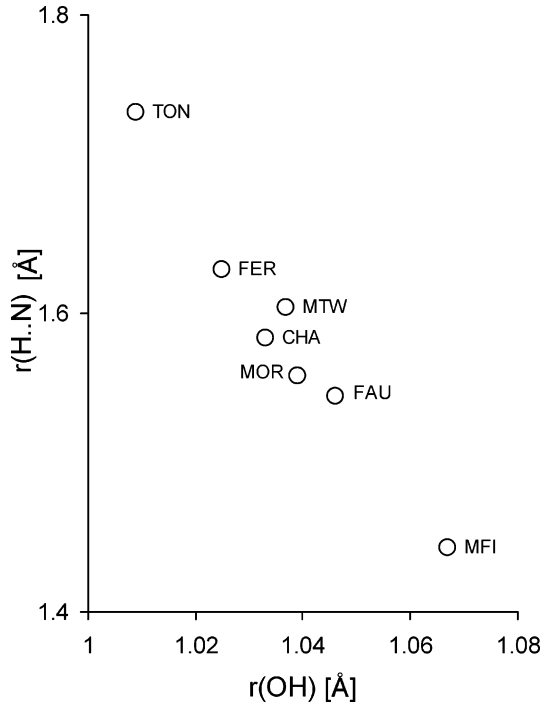

Figure 3. Distance r(OH) plotted versus hydrogen bond distance, r(H··N), as obtained from quantum chemical calculations.

the overall tendency of change for the Si−O−H angle is to lower values, whereas Al−O−H angles become larger.

The C≡N···H angle is a measure of the degree to which acetonitrile is tilted from the Al−(OH)−Si plane. For FAU, the least constrained system, this angle is at its largest value of 166°, indicating a preference for this near-linear configuration of the molecule with the framework proton. In our DFT cluster calculations, the starting positions of the acetonitrile were always taken from the results of the Monte Carlo Docking. The orientation of the acetonitrile is mainly dependent on the diameters of the channels or voids and on the curvature of the internal surface around the Brønsted site. The molecule will orientate in such a way as to minimize the repulsive interaction with the framework. In FAU and CHA, the two structures with cage-type voids rather than channels, the acetonitrile is orientated parallel to the 12 MR and 8 MR windows, respectively, and in CHA more tilted (due to steric constraint) from the Al−(OH)−Si plane than in FAU. In the case of CHA, our optimized geometry is very similar to one obtained by Trout et al.[44] from periodic Car-Parrinello simulations. Although it is not apparent that the same oxygen was protonated in that study, the orientation of the molecule with respect to the 8-ring and to the proton site in the P1 position of Trout et al. are very similar to ours, with their hydrogen bonding angles being slightly more linear (∠(C≡N···H) and ∠(N···H−O) respectively 165.4° and 172.4°, compared to 151.0° and 166.2° in this study). In MFI, MOR, and TON, we find the acetonitrile molecule orientated perpendicular to the main channel direction, roughly within the 10 or 12 MR plane. The observed tilting with respect to the Al−(OH)-Si plane stems from the attempt to approach the proton, which is not necessarily in the ring plane. Thus, we find quite different C≡N···H angles in MFI, MOR, and TON, though the molecules are found in the same type of position in the ring in all three cases. In FER and MTW, the molecule is oriented parallel to the main channel, i.e., roughly perpendicular to the 10 MR and 12 MR, respectively. The N···HO hydrogen bond angle is always between 178° and 161° which shows the preference of the nitrogen atom to lie close to the Al−(OH)−Si plane. In this way, we can think of the hydrogen bond as clearly being established between the lone electron pair of the nitrogen and the proton rather than between the π-electrons of the triple bond and the proton.

In terms of comparable experimental measurements, a number of infrared spectroscopic studies of d_3-acetonitrile in H-zeolites exist. The C≡N stretching frequency appears so far to offer little discrimination between different Brønsted sites. Wichterlova et al.[85] assigned bands at 2297 cm^{-1} to ν(C≡N) (shifted from 2265 cm^{-1} in the free molecule) in both FER(8.4) and MFI(12.6). Pazè et al.[47] found 2296 cm^{-1} in FER(8). The shift of the zeolite O−H stretch in the presence of acetonitrile has also been studied by a number of authors, although the situation is complicated by the splitting of the band. For instance Pazè et al.[47] found the ν(O−H) band in FER(Si/Al = 8) shifted from 3601 cm^{-1} in the unloaded zeolite to two peaks at 2870 and 2420 cm^{-1} upon sorption of CD_3CN. The splitting is caused by a Fermi resonance between the broadened hydroxyl band and the overtone of the in-plane hydroxyl bending, where the plane refers to that formed by Si−O−Al, as studied extensively by Meijer et al.[49,51] Jänchen et al.[53] calculated the center of gravity of the shifted bands after CD_3CN adsorption in a number of H-zeolites, finding 2500 cm^{-1} for MFI(52), 2540 cm^{-1} for MOR(10), 2560 cm^{-1} for MOR (6.7), 2590 cm^{-1} for FAU-(18), and 2680 cm^{-1} for FAU(5). Other factors being equal, one would expect stronger hydrogen bonding to result in a greater ν(O−H) shift, and from this point of view, these data are only partly consistent with our calculations. MFI(52) exhibits the strongest interaction, followed by MOR, as we predict from the hydrogen bonding geometries. If the frequency is taken as a measure of acidity, FAU remains the most weakly acidic, in contrast to our calculated results, though we note that frequency decreases with increasing Si/Al ratio.

3.4. Adsorption Energies. In Table 3, adsorption energies are also given. These were obtained by subtracting the total energies of the cluster (Z) and the acetonitrile molecule from the total energy of the cluster with acetonitrile adsorbed: $E_{ADS} = E_{ZA} - E_Z - E_A$. The adsorption energy can be thought of having three main components arising from the hydrogen bonding and from the electrostatic and short-range interactions between the molecule and the zeolite framework. The hydrogen bond interaction is the most important contribution as it holds the acetonitrile in place, but at the same time, the molecule will seek to maximize van der Waals' contact with the framework and to minimize repulsion. The extent to which it is able to do this will depend strongly on the local framework geometry and curvature. Therefore, a priori, we do not necessarily expect a correlation between the adsorption energy, E_{ADS}, and the hydrogen bond strength. Figure 4 shows a plot of the adsorption energy versus the r(OH) distance, from which it can be seen that MFI−A, the most acidic system, has a lower E_{ADS} than either FAU−A, MOR−A or MTW−A. The linear correlation coefficient including MFI in the series is 0.72, but without MFI 0.92, respectively. This reveals that E_{ADS} does in fact seem mainly to be governed by the strength of the hydrogen bond interaction. However, MFI is unusual in that it exhibits high acidity in the presence of acetonitrile, yet is a medium-pore 10-ring zeolite where steric constraints result in less than optimal short-range interactions with the molecule. As a comparison with the other systems having larger E_{ADS}, the channel diameters of these structures[99] are 5.5 × 5.1 Å for MFI, 7.4 × 7.4 Å for FAU, 6.5 × 7.5 Å for MOR, and 5.6 × 6.0 Å for MTW, respectively. Since the latter three are large-pore zeolites containing 12-membered rings, one would expect framework

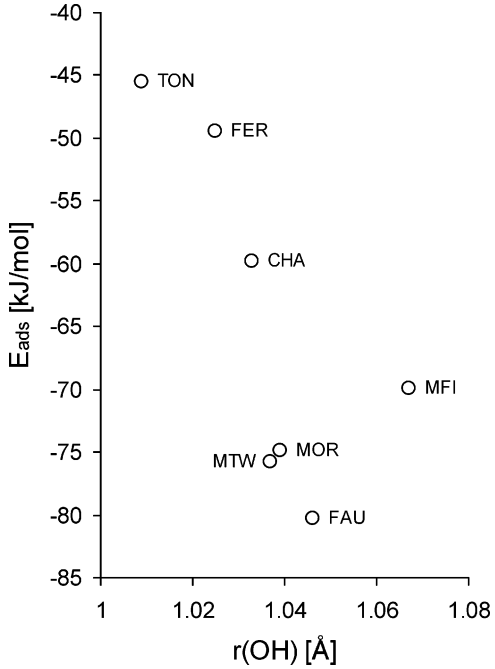

Figure 4. Plot of the adsorption energies versus the *r*(OH) distance, as obtained from quantum chemical calculations.

repulsive interactions to be greater for MFI, resulting in a reduction of the total E_{ADS}.

Experimentally, the differential heats of adsorption of acetonitrile in a variety of H-zeolites were determined by Yang et al.[100] These were MOR(Si/Al=40), MTW(280), FER(42), TON-(104), MFI(120) and CHA(80). At 400 K the differential heats for acetonitrile, across a range of coverage up to 1 molecule per acid site, were all in the region of 100 ± 10 kJ mol^{-1}. The authors concluded that the most likely reason for the heats being the same in all zeolites was that a molecule bound to an acid site would be unable to orient itself to maximize interactions with the cavity wall; that is, presumably the energy for physical adsorption (van der Waals' and electrostatic) in each case would be less than in the purely siliceous zeolite. Although there are dangers in comparing atomic-level quantum calculations with bulk calorimetric data, it can be seen that this interpretation is qualitatively consistent with our calculations in which we also predict the dominance of the hydrogen bonding in determining the adsorption energy. The difference lies in the fact that, in our static calculations, we have hydrogen bonds of different strength, whereas at 400 K, some of these differences may be averaged out by thermal motion and/or occupancy of other acid sites. Nevertheless, our calculations illustrate very well the tradeoff between optimal hydrogen-bonding geometry and physisorption which Yang et al.[100] suggest. Quantitatively, our energies are lower than those measured experimentally by some $20-50$ kJ mol^{-1}. In addition to the dispersive energy, which is not explicitly included in DFT calculations, long-range polarizing forces are also absent in our finite clusters, and together these two components could account for much of the discrepancy. In this regard, it is instructive to note that the Car-Parrinello study by Trout et al.,[44] carried out using a periodic model with one acid site per unit cell, and employing the PW91 functional with a plane wave basis set, yielded -68.4 and -72.1 kJ mol^{-1} as the energies of adsorption of acetonitrile at two different sites, compared to our value of -56.8 kJ mol^{-1}, suggesting a contribution of up to 16 kJ mol^{-1} from long-range terms. One should also consider the difference in vibrational zero-point energy, estimated as 8 kJ mol^{-1}, as well as the difference in kinetic energy from the ideal gas, formally 4RT,[44] although strictly a Monte Carlo sampling method should be used to evaluate the full distribution of states at finite temperature for meaningful comparison with measured heats.

4. Conclusions

Using different computational methods, we have investigated factors related to Brønsted acidity at representative acid sites in seven different high silica zeolites. We evaluated (i) the intrinsic acidity of the bare Brønsted sites using atomistic simulation methods and (ii) the acidity that is expressed when a molecule interacts with the Brønsted site by inserting acetonitrile in the zeolite structure and using quantum mechanical cluster calculations, using hydrogen-bond strength as a predictor of acidity. The selection of the Brønsted sites was based on a consistent scheme involving both the lattice energy of the structures and the accessibility of the site. We have chosen idealized structures with one Al per unit cell, as we wanted to investigate a whole range of zeolites, and using "real" Si/Al ratios leads to time-consuming studies of the Al distribution. The first approach to establishing a ranking of zeolites in order of intrinsic acidity was accomplished by calculating the ν(OH) stretching frequencies. We reinforced these findings by also calculating the gradient norm of the potential at the proton site, $|E|_H$. This describes the shallowness of the energy hypersurface at the proton: the smaller this is, the more easily the proton may be released, and thus the more acid the Brønsted site. We confirmed in our periodic models the strong correlation which exists between the two quantities, also proving the internal consistency of our calculations. The sequence in order of decreasing acidity, as inferred from the lattice energy and frequency calculations, is MFI > MOR > MTW > CHA > FER >TON > FAU. In general, agreement with experiment is reasonable in terms of proton siting, and of the overall trend of acidity. In the latter case we find FAU has the highest ν(OH) frequency, followed by MTW and MOR (where the proton sites are in the main 12-ring channels), in accordance with the widely perceived view that Brønsted acidity is lower in more open structures.

To study the acidity of a Brønsted site as encountered by a sorbate molecule, we investigated the hydrogen bond interaction between acetonitrile and the acid proton represented in a zeolite fragment (cluster) with quantum mechanical methods. In this case, we use the hydrogen bond geometry as a predictor of acid strength: a proton of strong acidity will be more easily donated into the hydrogen bonding causing a very strong interaction. We find an excellent correlation between the calculated *r*(O−H) bond length and the *r*(N··HO) hydrogen bond distance, and the *r*(O−H) bond length serves as a measure for hydrogen bond interaction strength. The sequence we found in order of decreasing H-bond strength was MFI > FAU > MOR > MTW > CHA > FER > TON. The Brønsted acid site in FAU is the most exposed of all of the investigated sites and allows the acetonitrile an approach without steric hindrance. The calculation of adsorption energies clearly reveals the two competing influences which govern the strength of adsorption: the attractive contribution of the hydrogen bond interaction and the more complex framework-acetonitrile interactions, which can either facilitate or hinder access to an acid site. We show that in all our zeolites, except MFI, the hydrogen bond interaction is dominant, as the sequence of adsorption energy is the same as that obtained from investigating the hydrogen bond strength. Comparing MFI to the three next most acid systems, FAU, MOR, and MTW, we see that MFI pores have smaller diameters,

and therefore, the acetonitrile likely experiences more repulsive short-range interactions, though the hydrogen bond is still by far the strongest component.

The calculations thus clearly illustrate the influence which pore topology may have on adsorption geometry and hence on hydrogen-bonding strength, though it is of note that (apart from the case of FAU already discussed) the actual ranking of the zeolites does not differ between the unloaded zeolites, characterized by ν(OH), and the hydrogen-bonded CH_3CN-containing systems. It may thus be argued that the intrinsic acidity is still a dominating factor in the zeolite−sorbate interaction, as evidenced by our calculations on the MFI structure, with the pore topology a secondary influence. In terms of the broad arguments, we might expect these two factors to oppose one another: intrinsic acidity is thought to be enhanced in more confined zeolite cavities, which conversely would act to hinder the approach of a bulky molecule to the active site. This could be further explored by considering other base molecules of larger size than acetonitrile. Quantitatively, our calculations do not always match up with experiment, though we have advanced a number of reasons why finite cluster calculations carried out with one acid site, and without consideration of temperature, may not exactly reproduce spectroscopic or bulk thermodynamic data. Overall though, using models of sufficient size to represent different pore structures, and a base of moderate strength, we have illustrated the subtle effects which different topologies may have on the acid chemistry of such materials. Our approach serves to demonstrate the utility of these computational methods in describing the strength and nature of the acid sites in zeolites and the complementarity of atomistic and quantum mechanical methods. The procedures are readily transferable to other zeolite types, Si/Al ratios and probe molecules, though some improvements in accuracy (at the expense of computational cost) may be gained through the deployment of embedded or periodic quantum methods, enabling the treatment of longer range interactions, as well as through the use of ab initio methods which allow some estimate of the dispersive forces.

Acknowledgment. The authors thank EPSRC and the Leverhulme Trust for financial support.

References and Notes

(1) Sierka, M.; Sauer, J. *J. Phys. Chem. B* **2001**, *105*, 1603.
(2) Baba, T.; Komatsu, N.; Ono, Y. *J. Phys. Chem. B* **1998**, *102*, 804.
(3) Chen, T.; Men, A.; Sun, P.; Zhou, J.; Yuan, Z.; Guo, Z.; Wang, J.; Ding, D.; Li, H. *Catal. Today* **1996**, *30*, 189.
(4) Sarv, P.; Tuherm, T.; Lippmaa, E.; Keskinen, K.; Root, A. *J. Phys. Chem.* **1995**, *99*, 13763.
(5) Shen, J.-P.; Sun, T.; Yang, X.-W.; Jiang, D.-Z.; Min, E.-Z. *J. Phys. Chem.* **1995**, *99*, 12332.
(6) Kramer, G. J.; van Santen, R. A. *J. Am. Chem. Soc.* **1993**, *115*, 2887.
(7) Schröder, K.-P.; Sauer, J. In *Proceedings of the 9th International Zeolite Conference*; von Ballmoos, R., Higgins, J. B., Treacy, M. M. J., Eds.; Butterworth-Heinemann: Boston, 1993; Vol. I, p 687.
(8) O'Malley, P. J.; Dwyer, J. *J. Phys. Chem.* **1988**, *92*, 3005.
(9) Eichler, U.; Brändle, M.; Sauer, J. *J. Phys. Chem. B* **1997**, *101*, 10035.
(10) Freude, D.; Ernst, H.; Wolf, I. *Solid State Nucl. Magn. Reson.* **1994**, *3*, 271.
(11) Fleischer, U.; Kutzelnigg, W.; Bleiber, A.; Sauer, J. *J. Am. Chem. Soc.* **1993**, *115*, 7833.
(12) Freude, D.; Klinowski, J.; Hamdan, H. *Chem. Phys. Lett.* **1988**, *149*, 355.
(13) Sillar, K.; Burk, P. *J. Mol. Struct. (THEOCHEM)* **2002**, *589*−*590*, 281.
(14) Zhao, Q.; Chen, W.-H.; Huang, S.-J.; Wu, Y.-C.; Lee, H.-K.; Liu, S.-B. *J. Phys. Chem. B* **2002**, *106*, 4462.
(15) Fuchs, A. H.; Cheetham, A. K. *J. Phys. Chem. B* **2001**, *105*, 7375.
(16) Haase, F.; Sauer, J. *Micropor. Mesopor. Mater.* **2000**, *35*−*36*, 379.
(17) Bonelli, B.; Civalleri, B.; Fubini, B.; Ugliengo, P.; Otero Areán, C.; Garrone, E. *J. Phys. Chem. B* **2000**, *104*, 10978.
(18) Kassab, E.; Jessri, H.; Allavena, M.; White, D. *J. Phys. Chem. A* **1999**, *103*, 2766.
(19) De Vries, A. H.; Sherwood, P.; Collins, S. J.; Rigby, A. M.; Rigutto, M.; Kramer, G. J. *J. Phys. Chem. B* **1999**, *103*, 6133.
(20) Civalleri, B.; Garrone, E.; Ugliengo, P. *J. Phys. Chem. B* **1998**, *102*, 2373.
(21) Barich, D. H.; Nicholas, J. B.; Xu, T.; Haw, J. F. *J. Am. Chem. Soc.* **1998**, *120*, 12342.
(22) Krossner, M.; Sauer, J. *J. Phys. Chem.* **1996**, *100*, 6199.
(23) Geobaldo, F.; Fiorilli, S.; Onida, B.; Giordano, G.; Katovic, A.; Garrone, E. *J. Phys. Chem. B* **2003**, *107*, 1258.
(24) Böhlmann, W.; Michel, D. *Top. Catal.* **2001**, *202*, 421.
(25) Nagano, J.; Eguchi, T.; Asanuma, T.; Masui, H.; Nakayama, H.; Nakamura, N.; Derouane, E. G. *Micropor. Mesopor. Mater.* **1999**, *33*, 249.
(26) Zholobenko, V. L.; Lukyanov, D. B.; Dwyer, J. *J. Phys. Chem. B* **1998**, *102*, 2715.
(27) Koller, H.; Meijer, E. L.; van Santen, R. A. *Solid State Nucl. Magn. Reson.* **1997**, *9*, 165.
(28) Blumenfeld, A. L.; Fripiat, J. J. *Top. Catal.* **1997**, *4*, 119.
(29) Haw, J. F.; Xu, T.; Nicholas, J. B.; Goguen, P. W. *Nature* **1997**, *389*, 832.
(30) Smith, L. J.; Davidson, A.; Cheetham, A. K. *Catal. Lett.* **1997**, *49*, 143.
(31) Hunger, M. *Solid State Nucl. Magn. Reson.* **1996**, *6*, 1.
(32) Chiche, B. H.; Dutartre, R.; Di Renzo, F.; Fajula, F. *Catal. Lett.* **1995**, *31*, 359.
(33) Wakabayashi, F.; Kondo, J. N.; Domen, K.; Hirose, C. *J. Phys. Chem.* **1995**, *99*, 10573.
(34) Biaglow, A. I.; Gorte, R. J.; Kokotailo, G. T.; White, D. *J. Catal.* **1994**, *148*, 779.
(35) Zholobenko, V. L.; Makarova, M. A.; Dwyer, J. *J. Phys. Chem.* **1993**, *97*, 5962.
(36) Hunger, B.; Heuchel, M.; Clark, L. A.; Snurr, R. Q. *J. Phys. Chem. B* **2002**, *106*, 3882.
(37) Onyestyák, G.; Valyon, J.; Rees, L. V. C. *Phys. Chem. Chem. Phys.* **2000**, *2*, 3077.
(38) Katada, N.; Kageyama, Y.; Niwa, M. *J. Phys. Chem. B* **2000**, *104*, 7561.
(39) Zhang, W.; Smirniotis, P. G.; Gangoda, M.; Bose, R. N. *J. Phys. Chem. B* **2000**, *104*, 4122.
(40) Zhang, W.; Burckle, E. C.; Smirniotis, P. G. *Micropor. Mesopor. Mater.* **1999**, *33*, 173.
(41) Brändle, M.; Sauer, J. *J. Am. Chem. Soc.* **1998**, *120*, 1556.
(42) Yin, F.; Blumenfeld, A. L.; Gruver, V.; Fripiat, J. J. *J. Phys. Chem. B* **1997**, *101*, 1824.
(43) Teunissen, E. H.; Jansen, A. P. J.; van Santen, R. A. *J. Phys. Chem.* **1995**, *99*, 1873.
(44) Trout, B. L.; Suits, B. H.; Gorte, R. J.; White, D. *J. Phys. Chem. B* **2000**, *104*, 11734.
(45) Gorte, R. J.; White, D. *Micropor. Mesopor. Mater.* **2000**, *35*−*36*, 447.
(46) Suits, B. H.; Šepa, J.; Gorte, R. J.; White, D. *J. Phys. Chem. B* **2000**, *104*, 5124.
(47) Pazè, C.; Zecchina, A.; Spera, S.; Spano, G.; Rivetti, F. *Phys. Chem. Chem. Phys.* **2000**, *2*, 5756.
(48) Smirnov, K. S.; Thibault-Starzyk, F. *J. Phys. Chem. B* **1999**, *103*, 8595.
(49) Meijer, E. L.; van Santen, R. A.; Jansen, A. P. J. *J. Phys. Chem. A* **1999**, *103*, 2553.
(50) Pazè, C.; Zecchina, A.; Spera, S.; Cosma, A.; Merlo, E.; Spanò, G.; Girotti, G. *Phys. Chem. Chem. Phys.* **1999**, *1*, 2627.
(51) Meijer, E. L.; van Santen, R. A.; Jansen, A. P. J. *J. Phys. Chem.* **1996**, *100*, 9282.
(52) Šepa, J.; Gorte, R. J.; White, D.; Kassab, E.; Allavena, M. *Chem. Phys. Lett.* **1996**, *262*, 321.
(53) Jänchen, J.; van Wolput, J. H. M. C.; van de Ven, L. J. M.; de Haan, J. W.; van Santen, R. A. *Catal. Lett.* **1996**, *39*, 147.
(54) Florián, J.; Kubelková, L. *J. Phys. Chem.* **1994**, *98*, 8734.
(55) Haw, J. F.; Hall, M. B.; Alvarado-Swaisgood, A. E.; Munson, E. J.; Lin, Z.; Beck, L. W.; Howard, T. *J. Am. Chem. Soc.* **1994**, *116*, 7308.
(56) Pelmenschikov, A. G.; van Santen, R. A.; Jänchen, J.; Meijer, E. *J. Phys. Chem.* **1993**, *97*, 11071.
(57) Simperler, A.; Mikenda, W. *Monatsh. Chem.* **1997**, *128*, 969.
(58) Cerius2 v.4.0; Accelrys Inc: San Diego, CA, 2000.
(59) Calligaris, M.; Nardin, G.; Randacchio, L.; Comin Chiaramonti, P. *Acta Crystallogr. B* **1982**, *38*, 602.
(60) Olson, D. H. *J. Phys. Chem.* **1970**, *74*, 2758.
(61) Vaughan, P. A. *Acta Crystallogr.* **1966**, *21*, 983.
(62) Olson, D. H.; Kokotailo, G. T.; Lawton, S. L.; Meier, W. M. *J. Phys. Chem.* **1981**, *85*, 2238.
(63) Alberti, A.; Davoli, P.; Vezzalini, G. *Z. Kristallogr.* **1986**, *175*, 249.

(64) Fyfe, C. A.; Gies, H.; Kokotailo, G. T.; Marler, B.; Cox, D. E. *J. Phys. Chem.* **1990**, *94*, 3718.
(65) Highcock, R. M.; Smith, G. W.; Wood, D. *Acta Crystallogr. C* **1985**, *41*, 1391.
(66) Cason, C. Persistence of Vision Ray Tracer, a.k.a POV−Ray; 3.1 g ed. Williamstown, Victoria, Australia, 1999.
(67) Foster, M. D.; Grey, A. E.; Lewis, D. W. *MAGIC*, Martin and Aileen's Gulp Input Creator, to be published.
(68) Gale, J. D. *J. Chem. Soc., Faraday Trans.* **1997**, *93*, 629.
(69) Schröder, K. P.; Sauer, J.; Leslie, M.; Catlow, C. R. A.; Thomas, J. M. *Chem. Phys. Lett.* **1992**, *188*, 320.
(70) Sanders, M. J.; Leslie, M.; Catlow, C. R. A. *J. Chem. Soc., Chem. Commun.* **1984**, 1273.
(71) Catlow, C. R. A.; James, R.; Mackrodt, W. C.; Stewart, R. F. *Phys. Rev. B* **1982**, *25*, 1006.
(72) Saul, P.; Catlow, C. R. A.; Kendrick, J. *Philos. Mag. B.* **1985**, *51*, 107.
(73) Freeman, C. M.; Catlow, C. R. A.; Thomas, J. M. *Chem. Phys. Lett.* **1991**, *186*, 137.
(74) Hill, J.-R.; Sauer, J. *J. Phys. Chem.* **1994**, *98*, 1238.
(75) Perdew, J. P.; Wang, Y. *Phys. Rev. B* **1986**, *33*, 8822.
(76) Hehre, W. J.; Ditchfield, J. A.; Pople, J. A. *J. Chem. Phys.* **1972**, *56*, 2257.
(77) Ugliengo, P.; Civalleri, B.; Zicovich-Wilson, C. M.; Dovesi, R. *Chem. Phys. Lett.* **2000**, *318*, 247.
(78) Brändle, M.; Sauer, J.; Dovesi, R.; Harrison, N. M. *J. Phys. Chem.* **1998**, *109*, 10379.
(79) Hill, J.-R.; Freemann, C. M.; Delley, B. *J. Phys. Chem.* **1999**, *103*, 3772.
(80) Sauer, J.; Eichler, U.; Meier, U.; Schäfer, A.; von Arnim, M.; Ahlrichs, R. *Chem. Phys. Lett.* **1999**, *308*, 147.
(81) Sierka, M.; Eichler, U.; Datka, J.; Sauer, J. *J. Phys. Chem. B* **1998**, *102*, 6397.
(82) Schröder, K.-P.; Sauer, J.; Leslie, M.; Catlow, C. R. A.; Thomas, J. M. *Chem. Phys. Lett.* **1992**, *188*, 320.
(83) Bordiga, S.; Turnes Palomino, G.; Pazè, C.; Zecchina, A. *Micropor. Mesopor. Mater.* **2000**, *34*, 67.
(84) Martucci, A.; Alberti, A.; Cruciani, G.; Radaelli, P.; Ciambelli, P.; Rapacciulo, M. *Micropor. Mesopor. Mater.* **1999**, *30*, 95.
(85) Wichterlová, B.; Tvaružková, Z.; Sobalík, Z.; Sarv, P. *Micropor. Mesopor. Mater.* **1998**, *24*, 223.
(86) Khaliullin, R. Z.; Bell, A. T.; Kazansky, V. B. *J. Phys. Chem. A* **2001**, *105*, 10454.
(87) Zygmunt, S. A.; Curtiss, L. A.; Iton, L. E.; Erhardt, M. K. *J. Phys. Chem.* **1996**, *100*, 6663.
(88) Brand, H. V.; Curtiss, L. A.; Iton, L. E. *J. Phys. Chem.* **1993**, *97*, 7.
(89) Demuth, T.; Hafner, J.; Benco, L.; Toulhoat, H. *J. Phys. Chem.* **2000**, *104*, 4593.
(90) Martucci, A.; Cruciani, G.; Alberti, A.; Ritter, C.; Ciambelli, P.; Rapacciuolo, M. *Micropor. Mesopor. Mater.* **2000**, *35*−*36*, 405.
(91) Alberti, A. *Zeolites* **1997**, *19*, 411.
(92) Boronat, M.; Zicovich-Wilson, C.; Viruela, P.; Corma, A. *Chem. Eur. J.* **2001**, *7*, 1295.
(93) Schröder, K.-P.; Sauer, J. *J. Phys. Chem.* **1996**, *100*, 11043.
(94) Sastre, G.; Lewis, D. W.; Corma, A. *Phys. Chem. Chem. Phys.* **2000**, *2*, 177.
(95) Lewis, D. W.; Sastre, G. *Chem. Commun.* **1999**, 349.
(96) Sastre, G.; Lewis, D. W. *J. Chem. Soc., Faraday Trans.* **1998**, *94*, 3049.
(97) Czyzniewska, J.; Chenevarin, S.; Thibault-Starzyk, F. *Stud. Surf. Sci. Catal.* **2002**, *142*, 335.
(98) Anderson, M. W.; Klinowski, J. *Zeolites* **1986**, *6*, 455.
(99) Baerlocher, C.; Meier, W. M.; Olson, D. H. *Atlas of Zeolite Framework Types*, 5th ed.; Elsevier: Amsterdam, 2001.
(100) Yang, L.; Trafford, K.; Kresnawahjuesa, O.; Šepa, J.; Gorte, R. J.; White, D. *J. Phys. Chem. B* **2001**, *105*, 1935.